A Diagnosis Approach for Typical Faults of Lithium-ion Battery Based on Extended Kalman Filter

Chao Wu[1,2,*], Chunbo Zhu[1], Yunwang Ge[2], Yongping Zhao[1]

[1] School of Electrical Engineering and Automation, Harbin Institute of Technology, Harbin 150001, People's Republic of China;
[2] Department of Electrical Engineering, Luoyang Institute of Science and Technology. Luoyang 471023, People's Republic of China;
[*]E-mail: shiningi@163.com

A fault diagnosis approach based on extended Kalman filter and incremental capacity analysis is proposed with fully understanding the internal failure mechanism of lithium-ion battery, which is extremely suitable for dynamic conditions. In order to detect and distinguish the fault modes and bridge fault symptoms with internal mechanisms, a serial of abusive experiments for over-discharge and low-temperature operation, which may commonly occur during battery applications, are arranged. Fault symptoms in form of electrical parameter variation are extracted as diagnosis basis. Furthermore, incremental capacity analysis is applied for isolation of the two similar faults. The diagnosis approach provides detailed description of symptoms and clear meaning of internal mechanisms. Post-disassembly analysis validates its reliability and effectiveness.

1. INTRODUCTION

As lithium-ion battery plays a more and more important role in wide applications due to its environmental friendliness, high power and energy density, its safety issue has caught increasing public concern. However, recent reported accidents during battery operation limit its further applications. Although lithium-ion battery is regarded as long service-life device, problems from manufacturing process and operating conditions may greatly degrade its performance, shorted its service life or even result in severe failure. So lithium-ion battery has faced an increased demand on reliability and safety. In one hand, researches on electrode material and manufacture process are

developed to provide cells with higher specifics; in the other hand, the management during operation is required to guarantee the performance and safety.

Fault diagnosis is a critical technique for battery application to detect successive performance degradation and abrupt fault [1-3]. More and more researches have been focused on this field. Sun provides a diagnosis system for lead acid battery packs with observation of charge/discharge curve changes, assuming the voltage curve under normal constant conditions is smooth [4]. Yufit uses X-ray computed tomography for post-mortem analysis of a failed lithium-ion polymer battery to quantification of the physical distortion [5]. Intelligent fault diagnosis system is also applied for battery [6, 7]. Liu [6] constructs a fuzzy fault diagnosis of battery and analyzes the relation between the data changes of battery external characteristics and the battery faults. Wu [7] also develops a battery fault expert diagnosis method based on fuzzy logic used for remote monitor and control system. Author in [8] proposes an adaptive fault diagnosis system for lithium-ion battery and construct nonlinear fault models with Kalman filter. These methods, however, have their limitations either because they can hardly be applied in situ or they fail to give a clear physical meaning for diagnosed fault modes. To our knowledge, the fault diagnosis approaches which connect external electrical characteristics with internal chemical process are rare, which will be the main topic in this paper.

1.1 Principle and Character of lithium-ion battery

In this section, we provide an overview on components of one typical lithium-ion battery and their internal mechanisms. Lithium-ion battery has anode and cathode as hosts for lithium ions. The anode is composed of a lithium intercalation compound, most commonly graphite, coated in a thin layer onto copper current collector. The cathode material, similar with anode, is powders coated in a thin layer onto aluminum. During charging process, the ions transfer from cathode and intercalate into anode; while reverse direction during discharge. Cell construction details, reactivity of cathode and anode may affect safety of entire cell. The separator between cathode and anode allows transfer of lithium ion and prevents the electrodes from direct contact. The separator will be "shutdown" at elevated temperature (usually 130-150°C) and melt at even higher temperature. Electrolyte provides a media for ion transport, which is usually composed of organic solvent and dissolved lithium salt. The current collector provides mechanical support for active material and transfer current throughout entire cell. The fundamental structure of lithium-ion battery is shown in Figure 1.
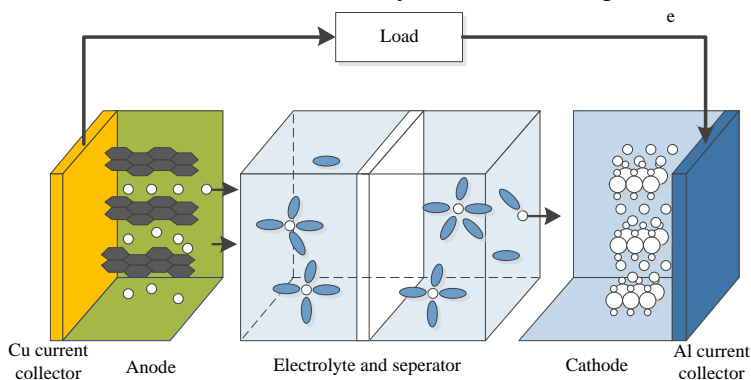

Figure 1. Structure of lithium-ion battery during discharge

1.2 Fault analysis of lithium-ion battery

Full knowledge of internal structure of lithium-ion battery helps us understand the internal mechanism of battery fault. In ideal case, only ion intercalation and de-intercalation at both electrodes occur which do not result in irreversible lithium consumption. However, side reactions and other processes at different components always take place with intercalation/de-intercalation and may be aggravated by abusive operation or terrible environment, such as thermal abuse (elevated temperature, low temperature), electrical abuse (overcharge, over-discharge, high-current rate) and mechanical abuse (nail penetration, crash). These processes destroy the equilibrium state shown in Figure 1 and induce irreversible consumption of lithium inventory or active material [9].

From the point of chemical view, internal causes of battery failure may result from:

(1) Phase change of cathode material;

(2) Lithium deposition at electrode, especially at anode;

(3) Electrolyte reduction;

(4) Solid electrolyte interface (SEI) decomposition at anode;

(5) Collector corrosion or dissolution;

(6) Separator penetration or melting.

However, during real applications, these internal mechanisms can not be detected directly. We can not dismantle a suspected cell in situ during operation to quantify the plated lithium at anode or the reduction of electrolyte. A bridge between internal chemical mechanisms and external electrical symptoms should be established for fault diagnosis of lithium-ion battery, as to say, detect the fault in form of measurable electrical parameters.

Well understanding the internal mechanisms connected with fault symptoms during battery fault process helps to establish a complete and accurate diagnosis system. In this paper, we focus on two fault modes which commonly occur during battery applications, especially during electric vehicle (EV) operation: (1) Dissolution of copper current collector due to over-discharge and (2) lithium plating at low temperature. First, we analyze the fault mechanisms for these faults to see what indeed happen inside the battery; then a serial of abusive experiments are carried out to extract external feature of related fault modes. Finally a fault diagnosis based on extended Kalman filter (EKF) and incremental capacity analysis (ICA) is achieved for fault diagnosis and isolation.

1.3 Fault modes

In this paper, we focus on two main fault modes which are discussed in this section.

(1) Dissolution of copper current collector due to over-discharge

Over-discharge hardly result in thermal runaway directly. However, electrochemically irreversible solid-state amorphization can be detected during deep over-discharge process which damages the host structure [10]. Once discharged below 1.5V, anodic dissolution of the current collector causes oxidization of Cu atoms to Cu^{2+} ions [11]. The dissolved copper may migrate through and penetrate the separator, resulting in a potential internal short. The case becomes even worse if the cell is driven into negative polarity and kept in that state temporarily. In this way thermal runaway may

occur during recharge process after deep over-discharge.

(2) Lithium plating at low temperature

Performance of lithium-ion battery at low temperature remains challenging today. Although low temperature discharging seems to cause little capacity loss, the main problem lies in that lithium plating becomes dominate during low temperature charging rather than intercalation at anode. Lithium plating occurs when the graphite potential is reduced below 0 V vs. Li/Li$^+$ or lithium-ion diffusion in the graphite particle is limited. Both conditions are aggravated with decreasing temperature. Furthermore, lithium plating induces a serious safety hazard that metallic lithium can grow dendritically at anode and has a potential to cause an internal short circuit [12, 13].

These two modes are discussed and compared because their internal mechanisms have similar manners, that is, both of their ion intercalation processes into anode are affected. In over-discharged case, the deposited copper may cover active area at anode and slow down intercalation. While during low-temperature operation, lithium plating also limits ion diffusion rate into anode. So it is meaningful to study their similarities and differences of behavior for early fault diagnosis and isolation.

2. EXPERIMENTAL SETUP

After understanding the internal mechanisms of mentioned faults, the abusive experiments for both faults are planned.

The commercial prismatic lithium-ion phosphate cells made in China are selected for study whose specifics are shown in table 1. Three cells for each fault were tested to extract the failure features and demonstrate reproducibility of the results, and average value of the three is reported here.

Table 1. Specifics of tested cell

Specifics	Values
Nominal capacity	40Ah
Cell dimension	46±1mm × 116±mm × 180.5±mm
Operating voltage range	2.5-3.65V
Temperature range	0-45°C
Weight	1.4±0.1Kg

All the tests were carried out in a temperature-controlled chamber. Arbin 2000 battery test system was used for conditioning and real-time parameter record. During standard cycling tests, cells were galvanostatically charged to 3.65V with 1C rate, followed by a potentiostatic charge at 3.65V until the current fell below C/20. The process is named as constant current, constant voltage charge mode (CC-CV mode). Discharging process was also galvanostatically with 1C until the voltage reached 2.5V.

Over-discharge Test (ODT): Over-discharge tests were carried out at 1C rate. All the cells were

charged with CC-CV protocol which was regarded as 100% state of charge (SOC) and discharged to 2.5V which was regarded as 100% depth of discharge (DOD). Then they were further discharged for an additional 10%SOC at C/25 to provide the presentation of the over-discharge performance. During ODT, we use as micro current-rate as possible to eliminate or minimize the joule heat generation so that it will not induce other fault mechanism.

Low temperature Test (LTT): Cycling from 2.5-3.65V with standard CC-CV protocol at -5°C.

Every ten cycles, the test was terminated and a full reference performance test was carried out to evaluate the current state of tested cell which contains a complete C/25 cycle, federal urban driving schedule (FUDS) and hybrid pulse power characteristic (HPPC) test. The cycle interval may be shortened as the performance degrades to a certain degree. The tests ended when a visible symptom occurs or the capacity of tested cell decreased to 60% of its nominal value.

3. FAULT DIAGNOSIS SYSTEM FOR LITHIUM-ION BATTERY

The basic idea of the fault diagnosis system lies in that we try to find a meaningful description for fault modes of lithium-ion battery in form of measurable parameter variations. As to say, a mathematical or electrical representation for battery is required.

3.1 Model of lithium-ion battery

During cycles of lithium-ion battery, the real-time data from sensors such as voltage, current and temperature will be obtained. Furthermore, some parameters related with internal chemical process should be calculated such as resistance or SOC. In this paper, we use Randles equivalent circuit model (ECM) to represent the behavior of a lithium-ion battery, which is shown in Figure 2. It is a simple but effective approach for parameter estimation. In this model, the voltage source stands for open circuit voltage(OCV) which usually depends on SOC and temperature, resistor Rs represents the total serial resistance (including resistor of electrolyte and connection), and parallel Rp//Cp network describes the time-dependent behaviors such as charge transfer and double-layer process.
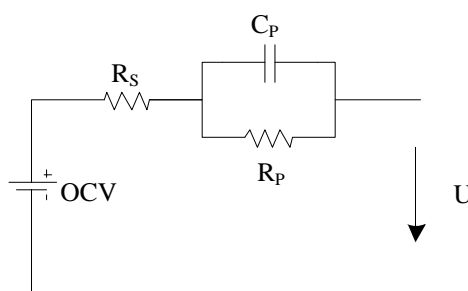

Figure 2. Equivalent circuit model of lithium-ion battery

3.2 Ageing experiments with typical fault mode

Feature extraction is the concentration of diagnosis system and it may directly affect diagnosis decisions. They must be able to describe the relationship between fault modes and symptoms mentioned above with clear physical meaning. In our system, reference performance test is performed regularly to extract the features during the complete degrading process. The variations of parameter in the ECM are treated as diagnosis basis. Here we provide the profiles of low-temperature tests as an example:
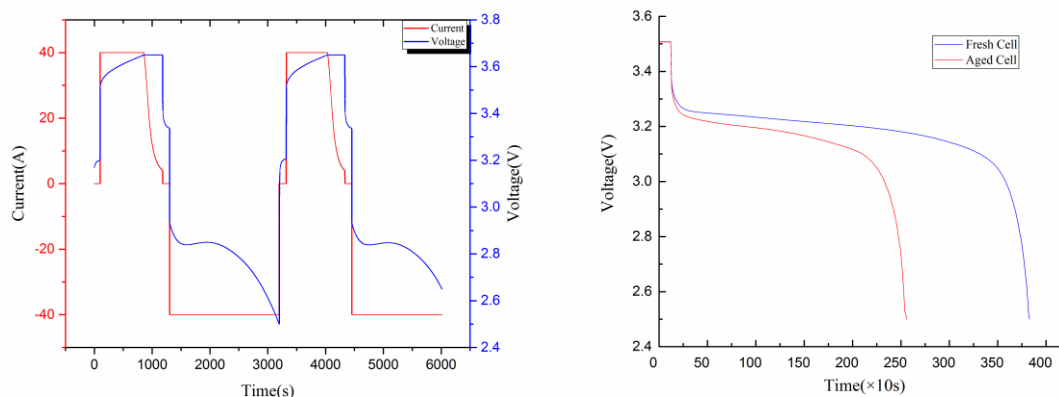

Figure 3. Profiles of battery with low-temperature operation a) Cycles at low temperature, b) discharge curves with different cycles

Figure 3 a) provides the fundamental profiles of voltage and current during operation at -5°C. The voltage curve during charge is a little different from normal operation. Constant current charging phase becomes shorter and constant voltage phase becomes dominate. This is because the polarization aggravates at low temperature. Also, abnormal voltage rise is observed during discharge and the new voltage platform can be explained by lithium plating. The overall capacity of the cell decreases with cycles. In Figure 3b), the discharge curves of fresh batteries and batteries after 100 cycles are compared. The capacity decreases from 40Ah to about 28Ah. So abusive factors such as low temperature indeed degrade performance of lithium-ion battery, and parameters mentioned in our model have to be derived to indicate the degradation.

3.3 Extended Kalman filter for parameter identification

Although parameters can be achieved through EIS or direct pulse test, a parameter extraction approach for dynamic condition is preferred due to real condition of battery applications [14]. Kalman filter induces state space to filter theory, and describes signal process with white noise through state equations. It estimates parameters and states of dynamic system using digital filter with LMS (least mean square). Kalman filter was first used for estimation of linear system, while Bucy, Sunahara extended it to nonlinear system, which is regarded as extended Kalman filter. It linearizes the nonlinear system with Taylor approximation and performs classic Kalman filter. The basic idea of EKF is shown

below [15].

State equations for nonlinear discrete system:

$$\begin{cases} x_{k+1} = f(x_k, u_k) + w_k \\ y_k = h(x_k, u_k) + v_k \end{cases}$$

Where, x_k is the system state vector, y_k is the system measurement vector, u_k is the input vector, $f(x_k, u_k)$ is the state transition function, $h(x_k, u_k)$ is the measurement function, w_k and v_k represent system noise and measurement error respectively and are independent with each other.

For nonlinear system, function $f(x_k, u_k)$ and $h(x_k, u_k)$ can be linearized by first order Taylor expansion:

$$\begin{cases} f(x_k, u_k) \approx f(\hat{x}_k, u_k) + \dfrac{\partial f(x_k, u_k)}{\partial x_k}\Big|_{x_k = \hat{x}_k} (x_k - \hat{x}_k) \\ h(x_k, u_k) \approx h(\hat{x}_k, u_k) + \dfrac{\partial h(x_k, u_k)}{\partial x_k}\Big|_{x_k = \hat{x}_k} (x_k - \hat{x}_k) \end{cases}$$

$\hat{x}_k$ is the estimated value for x_k, and the state equations can be rewritten as:

$$\begin{cases} x_{k+1} = \hat{A}_k x_k + \overbrace{f(\hat{x}_k, u_k) - \hat{A}_k \hat{x}_k}^{Bu_k} + w_k \\ y_k = \hat{C}_k x_k + \underbrace{h(\hat{x}_k, u_k) - \hat{C}_k \hat{x}_k}_{Du_k} + v_k \end{cases}$$

Where, $\dfrac{\partial f(x_k, u_k)}{\partial x_k}\Big|_{x_k = \hat{x}_k} = \hat{A}_k$, $\dfrac{\partial h(x_k, u_k)}{\partial x_k}\Big|_{x_k = \hat{x}_k} = \hat{C}_k$.

Back to our diagnosis system, we hope to use EKF estimate the real-time parameters for lithium-ion battery. We determine state vector as $x = (OCV, R_S, R_P, \tau, I_P)^T$, where R_S and R_P are parameters indicated in the ECM in Figure 2; input vector $u_k = I$ (current through the battery); system measurement vector $y_k = U$ (voltage across the battery); τ is the time constant of parallel network and equals to the product of C_P and R_P; I_P is the current flowing through the parallel resistor R_P.

Considering the discrete state equation of model listed in Figure 2:

$$\begin{cases} U_P((k+1)T) = \exp(-\dfrac{T}{\tau}) \times U_P(kT) + (1 - \exp(-\dfrac{T}{\tau})) \times I(kT) \times R_P \\ U(kT) = -U_P(kT) - I(kT)R_S + OCV \end{cases}$$

Where, U_P is the voltage across the parallel network, and we get:

$$\hat{A}_k = \begin{bmatrix} 1 & 0 & 0 & 0 & 0 \\ 0 & 1 & 0 & 0 & 0 \\ 0 & 0 & 1 & 0 & 0 \\ 0 & 0 & 0 & 1 & 0 \\ 0 & 0 & 0 & 0 & e^{-T/\tau} \end{bmatrix} \qquad B_k = \begin{bmatrix} 0 \\ 0 \\ 0 \\ 0 \\ 1 - e^{-T/\tau} \end{bmatrix}$$

$$\hat{C}_k = \begin{bmatrix} 1 \\ -I(kT) \\ -\dfrac{\partial(I_P(kT) \times R_P(kT))}{\partial R_P}\Bigg|_{R_P=R_P(kT)} \\ -\dfrac{\partial(I_P(kT) \times R_P(kT))}{\partial \tau}\Bigg|_{R_P=R_P(kT)} \\ R_P \end{bmatrix}^T \qquad D_k = [-R_S]$$

Process of parameter estimation for lithium-ion batteries is shown in Figure 4. *x(k/k-1)* is the result estimated according to previous state, *x(k-1/k-1)* is the optimal estimation of previous state while *P(k/k-1)* and *P(k-1/k-1)* are their corresponding error covariance. *G* is the Kalman gain which is used for updating the current optimal estimation *x(k/k)* from *x(k/k-1)*. *Q* and *R* are the covariance of system noise w_k and measurement noise v_k.
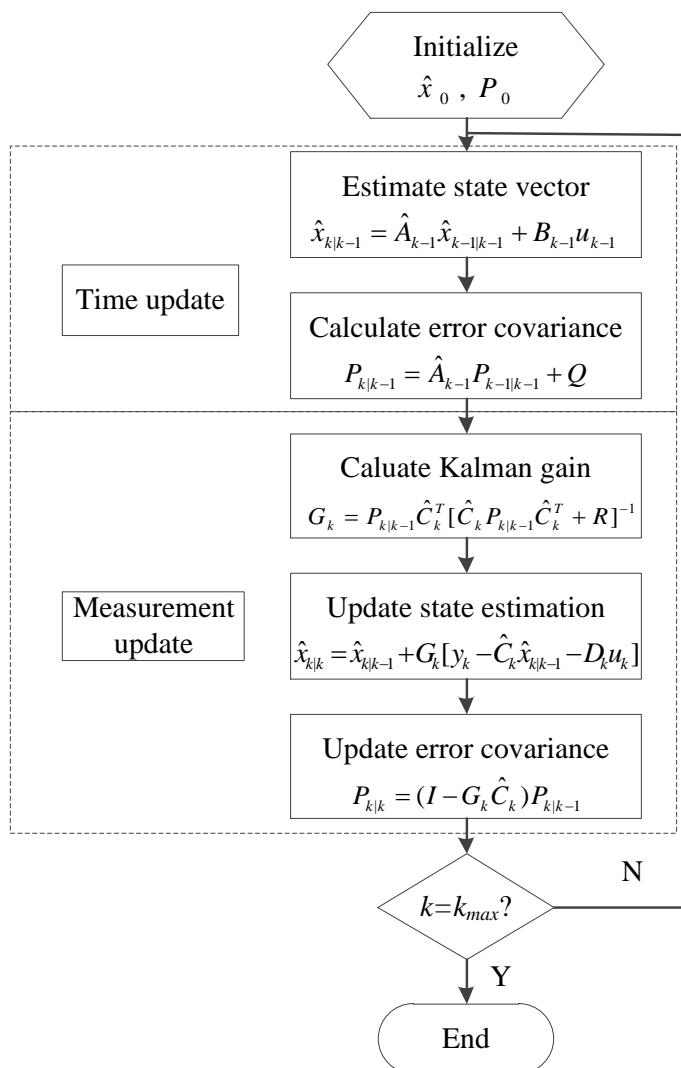

Figure 4. Process of extended Kalman filter

One fresh cell is taken for validation of the accuracy of EKF. The cell is operated under FUDS condition and its current and voltage are recorded. EKF is performed for parameter estimation whose results are shown in Figure 5 as well as the simulated R_S, R_P and time constant. The estimated voltage in Figure 5 agrees well with the measured one. Ignoring the error during the first cycle, the maximum error stays below 25mV and it always occurs at the transition moment from static state to dynamic state. During the operation, the simulation error could be further reduced to 15mV which indicates the accuracy of our parameter estimation for lithium-ion battery applications.
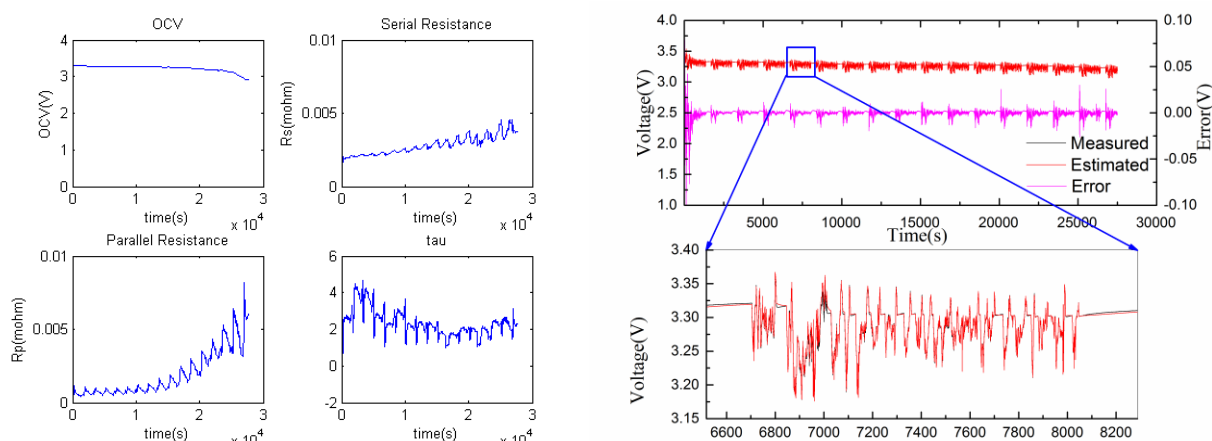

Figure 5. Simulation results of parameter estimation using EKF a) parameter estimation; b) comparison between measured and simulated voltage

The parameters from the fresh cell will be taken as reference. It means every time the parameters are extracted from a degraded cell, the parameters will be compared with the reference to tell if a fault occurs. As mentioned before, results are meaningful only if the comparison is made at the same environmental condition, i.e. the same voltage range and ambient temperature.

3.4 Incremental capacity analysis

Differential analysis has been reported for ageing mechanism explanation of lithium-ion battery. These curves can be used to elucidate phase transitions about the mechanism of the intercalation/de-intercalation of materials into electrodes. We can use either incremental capacity analysis (ICA) which comes from dQ/dV or differential capacity analysis (DCA) which refers to dV/dQ. Peaks in DCA curve represent phase transitions, while peaks in ICA curve represent phase equilibria. ICA is selected here and its curve could be obtained through low-rate constant current charge/discharge. Figure 6 provides a typical ICA curve of lithium-iron phosphate battery. This phase transformation between $FePO_4$ and $LiFePO_4$ at cathode is denoted as II. Phase transformations between C and LiC_x at anode are denoted as ①, ②, ③ and ⑤ respectively. So the peaks of a complete cell correspond to respective voltage platform during charge/discharge process and are denoted as ①II, ②II, ③II and ⑤II.
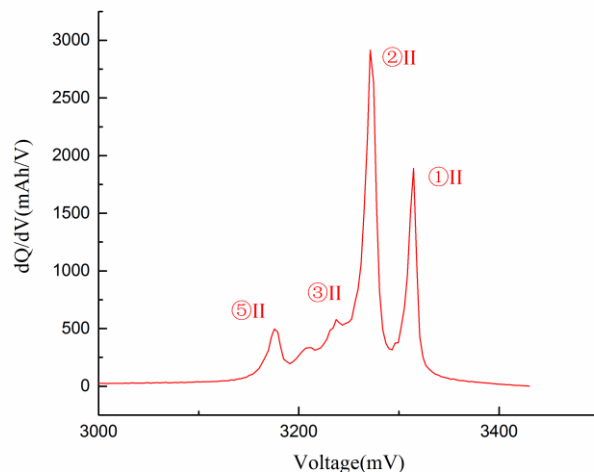
Figure 6. IC curve for a typical lithium-iron phosphate battery

4. SIMULATION AND DISCUSSION

Abused cells are brought out and tested under FUDS condition which simulated the real-world applications. Experiment results for comparison are provided in Figure 7. In Figure 7, cell 1 represents the average performance of the over-discharged cells and cell 2 is used for description of cells with low-temperature operation. The capacities of degraded cells are 28Ah and 31Ah, respectively, around 75% of their initial value. That means the cells suffer almost the same capacity degradation so the parameter variations extracted in this way will reflect the different mechanisms according to the different fault modes.
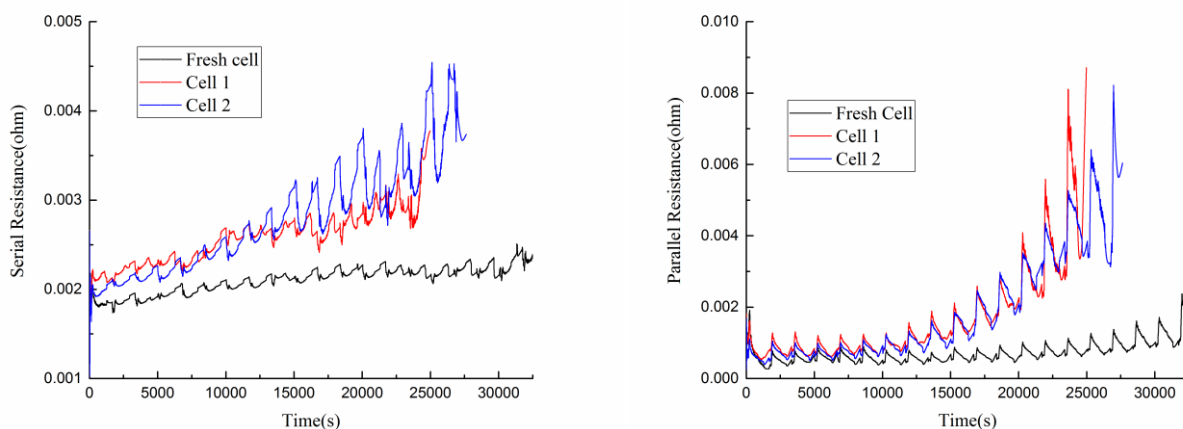

Figure 7. Comparison among parameter variation for different fault modes

Parameters of R_S, R_P and C_P vary in different manner, respectively during one FUDS cycle. Serial Resistances of both cell 1 and cell 2 increase; however, R_S of cell 1 is greater at SOC range of 70-100% and becomes smaller than cell 2 for rest of SOC range, which indicates a different dependency on SOC for different ageing mechanisms. R_P of both cells increase with almost the same rate, except for the end of discharge. The time constant of the battery in dynamic system, related with C_P, has the same dependency on SOC with reports in [19]. It always gets its minimum value at around 50-60% SOC. Over-discharge seems have less effect on time constant. Related fault is of ease to be diagnosed at SOC range from 30-65%, especially for R_P, where the parameter variation is obvious to be detected.

The experiment results are meaningful and reasonable. As we have mentioned before, over-discharge and low-temperature operation has some similar mechanism which limits the intercalation rate into anode. Although R_S shows a different dependency on SOC, the similar behavior makes it difficult to distinguish the two faults modes. Expert system with fuzzy logic may be a solution, but in this paper, we induce ICA for further diagnosis and isolation, whose results are shown in Figure 8.

IC curves of cell 1 and 2 are compared after abusive tests with fresh one. For cell 1, the peak denoted as ①Ⅱ, decreased its density with the other 3 peaks unchanged. The peak ②Ⅱ will decay only after ①Ⅱ completely disappear. However, for cell 2, both ①Ⅱ and ②Ⅱ degrade simultaneously and the other 2 peaks ③Ⅱ and ⑤Ⅱ seem to decrease their densities as well. This implies different mechanisms for the two fault modes that the electrodes of cell 1 were affected due to excessive loss of lithium and the main capacity loss may result from loss of active material. The process was not detected in cell 2; instead, the loss may be attributed to the successive loss of lithium inventory due to low temperature. The comparison gives us an approach to distinguish the two typical fault modes. Another observation is that all peaks of cell 1 and 2 move to a lower position and suggests an increase of battery resistance [21].
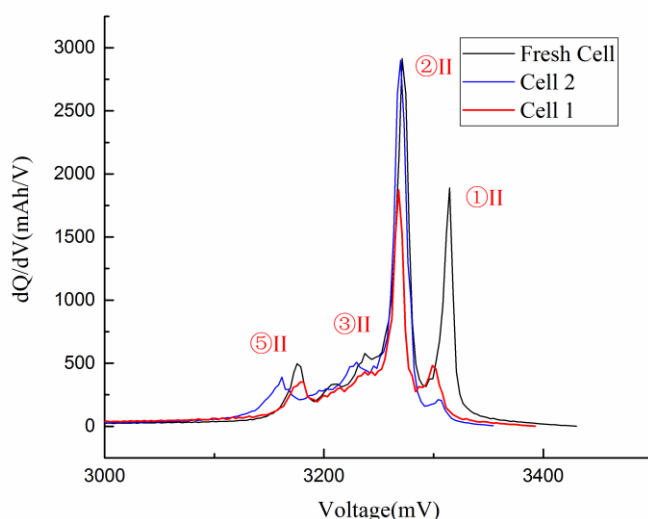

Figure 8. Comparison of ICA for different fault modes

In order to confirm the primary diagnosis results, a post-disassembly examination was followed. The aged cells were dismantled; anode and separator were examined respectively with direct observation and SEM. In Figure 9, we provide the evidence for each fault mode. Figure 9 a) showed the separator of cell 1 at cathode side. Certain residue on the separator could be observed which may be the mixture of deposited copper and oxidation products. For confirmation, XRD (X-ray diffraction) was applied here whose result was shown in 9 c). Existence of copper at cathode side indicates over-discharge results in current collect dissolution and migrates through separator. Furthermore, local separator became thinner which may suggest a potential micro short circuit. The active material was stripped from surface of anode which is not shown here. 9 b) represented anode of cell 2. Thin but uniform powders cover at the edge of anode, which is the reaction product of deposited lithium after exposed to air, and the lithium plating at low temperature is verified.
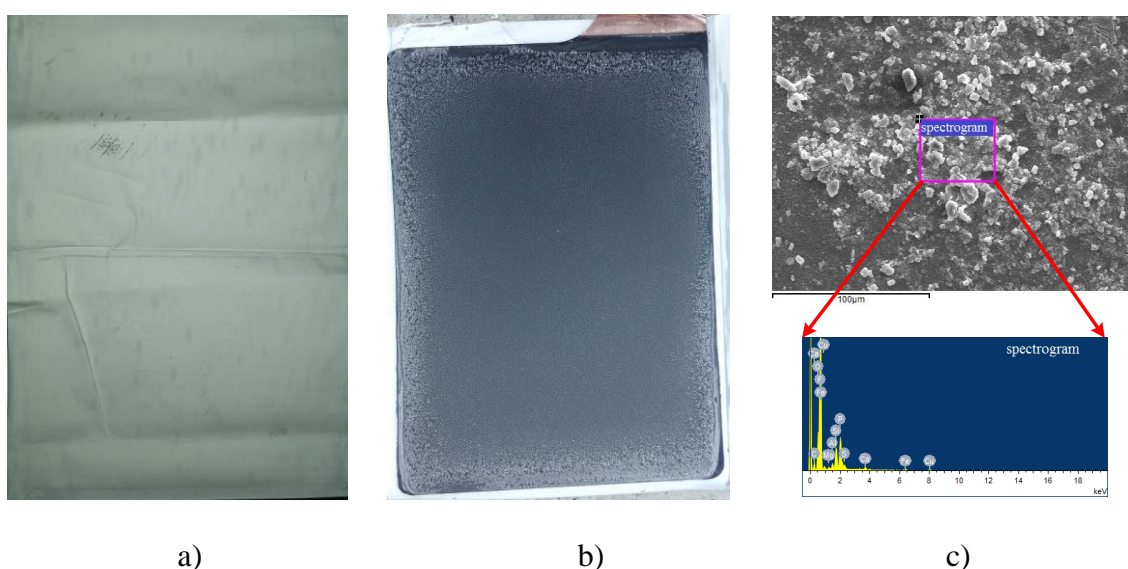

a)   b)   c)

Figure 9. Photographs of post-disassembly examination a) separator of cell 1, b) anode of cell 2, c) XRD of cell 1

5. CONCLUSION

It is important for lithium-ion battery applications to declare a "state of safety" as well as traditional SOC and SOH, which is related with performance degradation, module inhomogenity and potential fault. In this paper, a diagnosis approach for lithium-ion battery during applications is established based on EKF after fully understanding the fault mechanism. Abusive tests are performed to extract external parameter variation for each fault mode and try to establish a fault database in a measureable way. Two different fault mechanisms are evaluated. The similar tendencies of parameter variation serve as an indicator for fault occurrence and further fault isolation is achieved through ICA. Finally the diagnosis approach is validated with post-disassembly examination whose result shows the correctness and effectiveness of proposed approach.

However, due to the complexity of lithium-ion battery, more work could be done to improve our work. More fault modes should be added to complete the fault database; however, as the number of fault modes increases, the difficulty for isolation increases as well and the mutual relationship among different faults should be considered. Besides, real-time ageing process of battery will be added to system to tell the faults from normal degradation.

References

1. U. Troltzsch, O. Kanoun and H. S. Trankler, *Electrocihimica Acta*, 51, (2004) 1664-1672.
2. L.G. Lu, X.B. Han and J.Q. Li, *Journal of Power Sources*, 226 (2013) 272-288.
3. S.L. Wang, L.P. Shang, Z.F. Li, H. Deng and Y.L. Ma, *International Journal of Electrochemical Science*, 10 (6) (2015) 5130-5151.
4. Y.H. Sun, H.L. Jou, J.C. Wu and K.D. Wu, *Applied Energy*, 87 (2010) 3691-3698.
5. V. Yufit, P. Shearing, R.W. Hamilton, P.D. Lee, M. Wu and N.P. Brandon, *Electrochemistry Communications*, 13 (2011) 608-610.
6. W.J. Liu, "Research and implementation of failure diagnosis expert system for battery pack," Master dissertation, Hunan University, 2005.
7. J.R. Wu, "Design of remote monitoring system and study on fault diagnosis method for electric vehicle," Master dissertation, Jilin University, 2011
8. A. Sidhu, A. Izadian and S. Anwar, *IEEE Transactions on Industrial Electronics*, 62(2) (2015) 1002-1011.
9. 9. C. Wu, C.B. Zhu, Y.W. Ge, Y.P. Zhao, *Journal of Nanomaterials*, 631263 (2015).
10. H. Maleki and J.N. Howard, *Journal of Power Sources*, 160 (2006) 1395-1402.
11. T.C. Kaypmaz, D. Uzun and R.N. Tuncay, "Analysis of Over Charge & Over Discharge Characteristics and Failure Detection of Li-ion Polymer Batteries," presented at the 4th International Conference on Automotive Technologies, Istanbul, Turkey, 2008.
12. M. Petzl, M. Kasper and M.A. Danzer, *Journal of Power Sources*, 275 (2015) 799-807.
13. M. Petzl, M.A. Danzer, *Journal of Power Sources*, 254 (2014) 80-87.
14. Y.J. Zheng, X.B. Han, L.G. Lu, J.Q. Li and M.G. Ouyang, *Journal of Power Sources*, 223 (2013) 136-146.
15. N. Galushkin, N. Yazvinskaya and D. Galushkin, *International Journal of Electrochemical Science*, 9 (11) (2014) 6305-6327.
16. C. Hua, B.D. Youn and J. Chung, *Applied Energy*, 92 (2012) 694–704.
17. I. Bloom, A.N. Jansen, D.P. Abraham, J. Knuth, S.A. Jones, V.S. Battaglia and G.L. Henriksen, *Journal of Power Sources*, 139 (2005) 295–303.
18. X.B. Han, M.G. Ouyang, L.G. Lu, J.Q. Li, Y.J. Zheng and Z Li, *Journal of Power Sources*, 251 (2014) 38-54
19. W. Waag, S. Käbitz and D.U. Sauer, Applied energy, 102 (2013) 885–897.
20. A. Widodo, M.C. Shim, W. Caesarendra and B.S. Yang, *Expert Systems with Applications*, 38 (2011) 11763–11769.
21. M. Dubarry, B.Y. Liaw, M. Chen, S. Chyan, K. Han and W. Sie, S. Wu, *Journal of Power Sources*, 196 (2011) 3420-3425.